APPARATUS AND DEMONSTRATION NOTES

Jeffrey S. Dunham, *Editor*
Department of Physics, Middlebury College, Middlebury, Vermont 05753

This department welcomes brief communications reporting new demonstrations, laboratory equipment, techniques, or materials of interest to teachers of physics. Notes on new applications of older apparatus, measurements supplementing data supplied by manufacturers, information which, while not new, is not generally known, procurement information, and news about apparatus under development may be suitable for publication in this section. Neither the *American Journal of Physics* nor the Editors assume responsibility for the correctness of the information presented. Submit materials to Jeffrey S. Dunham, *Editor.*

A vision-based motion sensor for undergraduate laboratories

Edcel John Salumbides,[a] Joyce Maristela, Alfredson Uy, and Kees Karremans
Physics Department, University of San Carlos, Cebu City, Philippines

(Received 1 February 2001; accepted 12 October 2001)

[DOI: 10.1119/1.1427312]

I. INTRODUCTION

Most undergraduate physics laboratory courses start with mechanics experiments. Well-known examples such as the simple pendulum, free fall, and coupled pendulum experiments are usually among the first experiences. An essential part of these experiments is converting the motion of a three-dimensional object to a one-dimensional position–time graph. The experiment is usually designed in such a way that the amount of measured data is reduced. Experiments measuring the gravitational acceleration g, such as the simple pendulum experiment and the free-fall experiment, illustrate this process of data reduction. In the simple pendulum experiment, the quantity of interest, the period of oscillation, can be measured with a simple stopwatch. In combination with the length of the pendulum, this result yields the value for g. In the free-fall experiment, theory shows that three position–time coordinates are sufficient to determine g. In both experiments, theory shows that the dynamic behavior of the system can be determined by a small number of measurements. The experiments are designed so that these measurements are recorded and not the motion of the object itself.

Recently a more general approach has been developed in order to investigate the mechanics of moving objects. In this method, the motion is recorded with a video camera, hence data reduction can be performed with a computer after recording. Using commercial software like VideoPoint, the position of the object is determined by pointing the mouse at a reference point on the moving object in each frame of the recorded video.[1] This procedure is not only time-consuming, it also introduces significant errors into the measurements of the position. A more thorough investigation of this method has revealed a second problem. The time interval between consecutive frames is not constant, introducing small random errors in timing, a problem that seems to be hard to circumvent when using a video camera.

In this paper we describe an alternative method in which the use of computer vision algorithms results in a more accurate determination of the position of the moving object. To avoid the timing problem inherent with the use of a video camera, we opted for a charge-coupled device (CCD) camera as the recording device. In combination with a user-friendly calibration interface, our vision-based motion sensor promises to become an accurate method that can be applied to a wide range of experiments.

II. DESIGN AND IMPLEMENTATION

We have developed a motion sensor that records the motion of an object with a CCD camera. A computer program has been written to analyze the recorded motion of the object. In the first part of our method, we record images separated by a fixed time interval. The rate at which the pictures can be stored in the computer is limited by the configuration of the image acquisition card used. In the second part, the sequence of images is analyzed. Postponing this time-consuming analysis task reduces the requirements on the computer used. By avoiding real-time data analysis, a personal computer turns out to be capable of running our program.

The CCD camera (Watec LCL-903HS) is coupled to the computer via the IMAQ PCI-1408 image acquisition device (National Instruments). The program was developed in the LABVIEW programming language using routines from the IMAQ library.[2,3] The LABVIEW environment provides libraries that enable one to combine image-grabbing and image-processing without switching application software. This feature is much simpler than using C or FORTRAN routines for which one would need interfacing programs.

A. Image acquisition

The CCD camera images are separated in time by a specified interval. The successive snapshots of an object in motion are stored as bitmap (BMP) files that are labeled chronologically. Since the accurate measurement of the time interval between captured images is essential for further analysis, we performed a test to see if timing was done consistently. We recorded subsequent images of the display of a digital counter and observed that irregular time intervals occurred between successive images. This problem was eliminated by

 © 2002 American Association of Physics Teachers

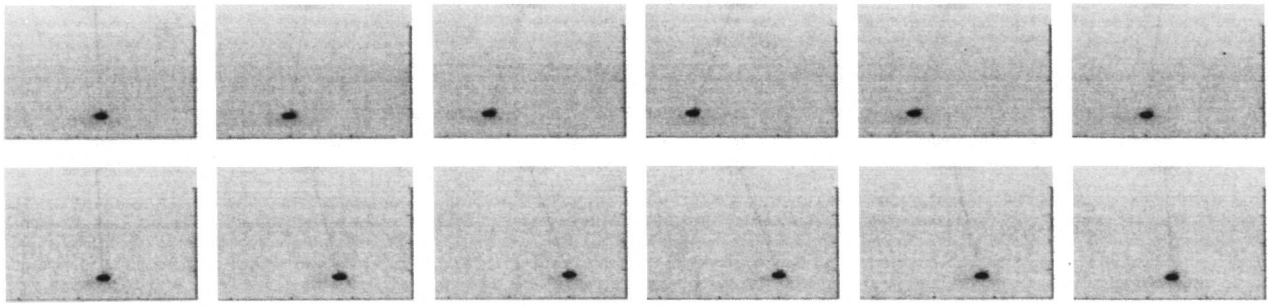

Fig. 1. A sequence of images taken over one period of the pendulum.

triggering the IMAQ card externally using a function generator; a constant time interval between consecutive images was then observed.[4] The time interval in our measurements was set at 112 ± 1 ms, the minimum time interval for which the IMAQ card can acquire successive images.

B. Data processing

The image analysis routine generates a list of coordinates of the moving object expressed in physical units, i.e., meters. Several computer vision algorithms are implemented to trace the trajectory of the object's center of mass for the complete sequence of images. We have divided the process into three subroutines: calibration, object detection, and tracking.

In the calibration subroutine, we determine the conversion factor for transforming the position coordinates expressed in pixel units to units of length. In this procedure, an object of known length in the image is used to determine the actual spacing between pixels. The first frame in the sequence is used to obtain the conversion factors in the horizontal and vertical directions. For our CCD images the calibration factor in the vertical direction is twice the calibration factor in the horizontal direction. These conversion factors are then used for the other frames.

For object detection, the subroutine has to identify the cluster of pixels that represents the object under investigation. In general, experiments can be set up in such a way that the object of interest can be distinguished easily from the background. We have used a thresholding algorithm for this purpose. Thresholding is the process of converting a grey-level image into a bi-level image by specifying a threshold value.[5] Pixel values above the threshold value are assigned to a region indicated by the value 1; the other pixels are assigned to the region indicated by the value 0. IMAQ provides routines for the automatic determination of the threshold that gives satisfactory results. After the thresholding operation, the images exhibit some distortions in the form of horizontal lines extending in the direction of motion. This effect results from the image acquisition process. The lines are scanned horizontally, starting with the odd-numbered lines, followed by the even-numbered ones. Since the object moves, the lines are scanned with the object at different positions, resulting in the observed phenomena.[2] The distortions have an intensity value different from that of the region representing the object, causing pixels from the background to appear within the object region. The spurious background pixels have the effect of fragmenting the object into several separate regions. To eliminate this problem, a spatial filter is used prior to the thresholding process. In the spatial filtering routine, the pixel values are replaced by the average intensity values of the neighboring pixels.[6]

In the tracking subroutine, the geometric center of the object is located in every image of the sequence. The geometric center can be determined using the centroid function provided by IMAQ. This function determines the pixel coordinates of the center of the object.[7,8]

The x and y coordinates of the object's center of mass are recorded for each image. Using the conversion factors from the calibration routine we convert the position values into real physical units. We then transform the data into a position–time graph that represents the object's motion.

III. EXPERIMENTAL RESULTS

We used the vision-based motion sensor in two experiments and compared its performance with that of conventional procedures. In the first experiment we measured the period of a simple pendulum. In the second experiment we determined the terminal velocity of a falling balloon. The results from these experiments provide insight into the accuracy of the position and time measurements obtained using the vision-based motion sensor.

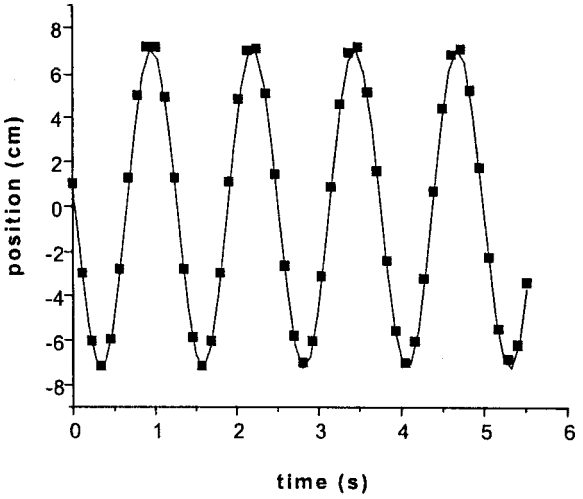

Fig. 2. The horizontal position of the pendulum with respect to its equilibrium position as a function of time. The center-of-mass measurements are represented by the points. The period of the pendulum was obtained from the sinusoidal fit shown as the superimposed curve.

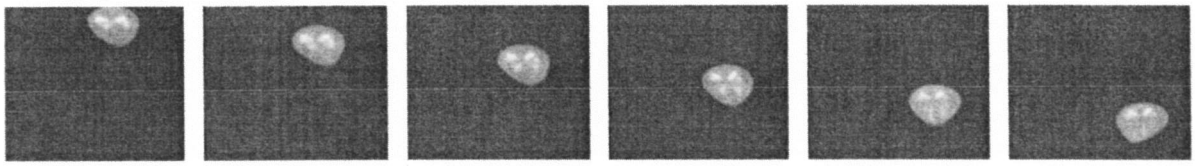

Fig. 3. Six consecutive images of a falling balloon with an effective mass of 3.2 g. The time interval between the images is 112.5 ms.

A. Pendulum motion

The simple pendulum consisting of a bob attached to a cord was designed in such a way that the pendulum bob appeared darker than the background. A ruler with centimeter markers was used for calibration purposes. The camera was oriented perpendicular to the plane of motion. We acquired a sequence of 50 images, some of which are shown in Fig. 1. In this experiment, the geometric center of the pendulum bob coincides with its center of mass. In Fig. 2, the horizontal position of the center of mass with respect to its equilibrium position is plotted against time. The data points were fitted using a sinusoidal function, from which the period was determined to be 1.243 ± 0.001 s. Using a stopwatch to measure the period gave a value of 1.3 ± 0.1 s, while with the rotary motion sensor, a period of 1.25 ± 0.01 s was obtained. The different experimental methods for determining the period are in good agreement with each other. The results also show that the vision-based motion sensor offers improved accuracy over conventional methods.

B. Terminal velocity

We followed the suggestion from Takahashi and Thompson of using balloons for the terminal velocity experiment.[9] Balloons are particularly suited for these types of experiments because they reach their terminal velocity in a short time. In this experiment we have investigated the relationship between the force of air resistance and velocity of the balloon.

The motion of a falling object of mass m which experiences the force of air resistance $f(v)$ is described by

$$m\frac{dv}{dt} = m_{\text{eff}}\, g - f(v), \tag{1}$$

where m_{eff} is the effective mass of the object taking into account the buoyancy force exerted by the displaced air.[9] The terminal velocity v_T is achieved when the force of air resistance balances the apparent weight, that is, when

$$f(v_T) = m_{\text{eff}}\, g, \tag{2}$$

resulting in zero acceleration. The effective mass of the balloon was measured with a balance where it experiences the same buoyancy force as in the experiment. The terminal velocity depends on the effective mass of the falling body; therefore, changing the effective mass of the balloon by attaching different masses provides the means to investigate the relationship between the force of air resistance and the terminal velocity. In this experiment, we investigated whether the relationship between the force due to air resistance and velocity was linear or quadratic.

The set-up used for the pendulum experiment was modified slightly for the experiment on the balloon. The balloon is highly reflective compared to the dark bob used in the pendulum experiment. A dark background was therefore used in this experiment in order to enhance the contrast between the balloon and the background.

Figure 3 shows some captured images. We used the position coordinates of the geometric center obtained from the tracking subroutine. The position–time graph obtained from the sequence is shown in Fig. 4. The linear relationship between the vertical position and time shows that the balloon has reached its terminal velocity. Figure 5 shows the data for the terminal velocity as a function of the effective mass.

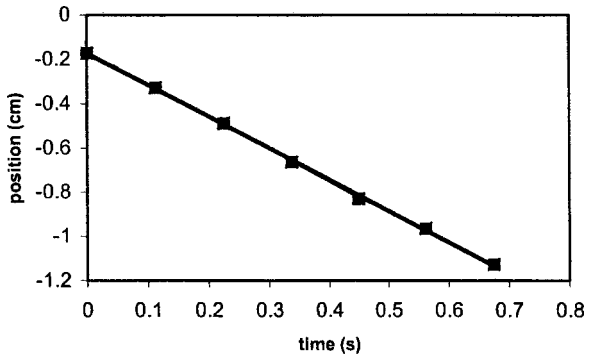

Fig. 4. The position–time graph of a falling balloon with an effective mass of 3.2 g. The linear fit shows that the balloon has reached its terminal velocity.

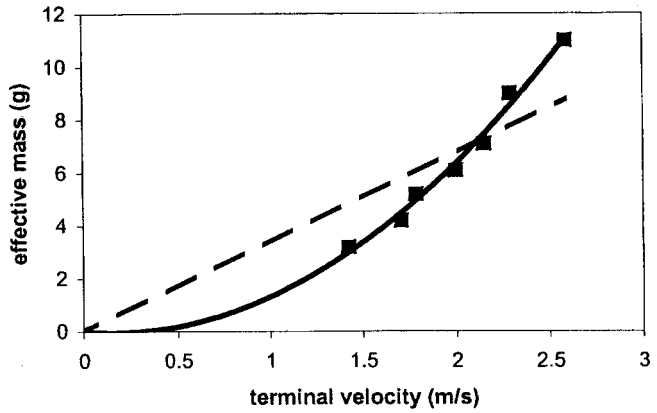

Fig. 5. The terminal velocity of the balloon for different effective masses. The rectangular points are the data points obtained from the experiment. The curve shows a fit to a quadratic function (solid curve) and a linear function (dashed line).

When the data are fitted with a quadratic function this experiment provides clear evidence that the force of air friction increases with the square of the velocity.

IV. CONCLUSION

The computer vision techniques used in the vision-based motion sensor offer clear advantages over commercially available software such as VideoPoint. Our fully automated tracking of the object takes over the time-consuming task of indicating the position of the object on every frame. This makes the procedure not only faster, it also results in more accurate position values. Compared to other sensors the values obtained with the vision-based motion sensor have greater accuracy. In addition to the improvement in accuracy the method has the benefit of flexibility. Applying only slight modifications, the vision-based motion sensor showed its potential in experiments on the simple pendulum and free-falling balloon.

The sensor is not restricted to recording the motion of a single object. The motion sensor can also be used to study the motion of two-body systems. Small changes in the program can be made in order to study the dynamics of a coupled pendulum. We believe that the vision-based motion sensor, which combines the flexibility of commercial software with the accuracy of a dedicated motion sensor, is a useful tool in undergraduate laboratories.

[a]Electronic mail: ejlsalumbides@hotmail.com

[1]VideoPoint®, designed for use with Windows and Macintosh operating systems is published by Lenox Softworks and distributed by PASCO scientific. For more information, visit www.lsw.com\videopoint.
[2]LABVIEW® User Manual, U.S.A., 1996, pp. 9-1–20-10.
[3]IMAQ™ Vision for G Reference Manual, U.S.A., 1997, pp. 9-1–19-20.
[4]Getting Started with your IMAQ PCI/PXI 1408 and the NI-IMAQ™ Software for Windows 95/NT, U.S.A., 1997, pp. 3–4.
[5]R. J. Schalkoff, *Digital Image Processing and Computer Vision* (Wiley, Singapore, 1989), pp. 178–179.
[6]E. R. Davies, *Machine Vision: Theories, Algorithms, Practicalities* (Academic, London, 1990), pp. 42–44.
[7]R. C. Gonzalez and R. E. Woods, *Digital Image Processing* (Addison–Wesley, Reading, MA, 1993), pp. 514–517.
[8]J. R. Parker, *Practical Computer Vision Using C* (Wiley, New York, 1994), pp. 56–59.
[9]K. Takahashi and D. Thompson, ''Measuring air resistance in a computerized laboratory,'' Am. J. Phys. **67**, 709–711 (1999).

Modeling the electrical resistivity of the earth's subsurface on paper

K. G. Vandervoort,[a] M. J. Lesmerises,[b] K. C. Shuler, and J. M. Spratt
Department of Chemistry and Physics, Western Carolina University, Cullowhee, North Carolina 28723

(Received 9 September 2001; accepted 13 February 2002)

[DOI: 10.1119/1.1467910]

I. INTRODUCTION

We describe a laboratory experiment that models a resistivity survey of the earth, a noninvasive technique commonly used by geophysicists to investigate the shallow subsurface. Others have reported the implementation of a geophysical resistivity lab into an undergraduate physics course.[1–3] There are several differences between the experiment we describe here and previously published work. Our experiment uses common off-the-shelf equipment including voltmeters, power supplies, and conducting paper, and does not require the construction or purchase of new equipment. In a standard resistivity field experiment, one instrument is shared among a class of students. In our indoor experiment, each pair of students has its own setup and is involved in all aspects of data collection and analysis. In addition, the depth of each layer can be changed readily and its effects observed, both on the measured resistivity and on the distribution of the current density. Also, analysis of the two-dimensional paper model is somewhat simpler than the three-dimensional field model. Both horizontal and vertical layering are investigated, and results are obtained that are qualitatively equivalent to an actual geophysical survey.

For simplicity, we model the resistivity of the earth using the Wenner electrode spread.[4] This electrode spread is commonly employed by geophysicists and is characterized by an equal spacing between adjacent electrodes. (For example, see Fig. 1.) The outer two electrodes are connected to a variable power supply and the current is held constant. The electric potential difference between the inner two electrodes is then measured to determine the resistivity of the ground. To derive the resistivity for a homogeneous subsurface using a Wenner electrode spread, one applies Ohm's law and the definition of the electric field as the gradient of the electric potential to an infinite hemisphere.[4] The result of this derivation is that the electric potential difference (ΔV) between the inner two electrodes is determined by $\Delta V=\rho I/2\pi a$, where a is the spacing between electrodes, ρ is the resistivity, and I is the current. When modeling a Wenner electrode spread on a paper of thickness t, the situation is changed from an infinite hemisphere to an infinite half-circle. The result in this case, $\Delta V=(\rho I/\pi t)\ln(4)$, is similar mathematically to a geophysical spread that uses line rather than point electrodes.[5] The important feature of this result is that the electric potential difference between the inner two electrodes is independent of the a-spacing, making the analysis more straightforward and thus allowing the student to see changes in the electric potential difference that directly reflect the resistivity of the subsurface layers without requiring a correction for the a-spacing.

For an inhomogeneous subsurface, as occurs for the case of multiple horizontal layers of different resistivities, the analysis of the measured resistivity is much more complicated.[4] Using the expressions above, the measured potential is converted into an *apparent* resistivity, which is a weighted average of the resistivities of the multiple layers. The purpose of our experiment is to demonstrate that the resistivity of subsurface layers can be measured, and to mea-

 © 2002 American Association of Physics Teachers

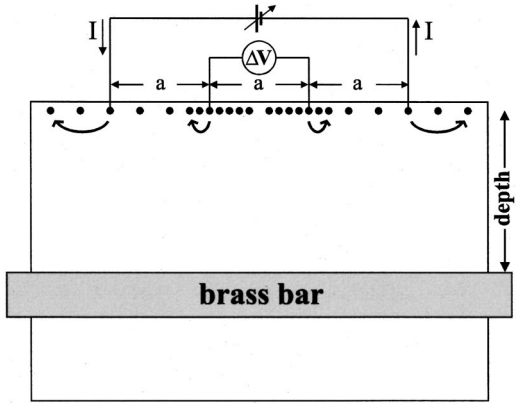

Fig. 1. Four electrode Wenner spread on paper with adjustable brass bar. The power supply (represented as a variable battery) is attached to the outer two electrodes and the current is held constant in this section of the circuit. The electrical potential difference (labeled ΔV) between the inner two electrodes is measured. To accommodate other *a*-spacings, all four electrodes are moved, keeping the center of the electrode spread stationary. For example, the curved arrows indicate how the spread would be relocated from its present location (for an *a*-spacing of 10 cm) to a different location (for an *a*-spacing of 14 cm). Pushpin locations (closed circles) facilitate *a*-spacings of 2, 4, 6, 8, 10, 12, and 14 cm.

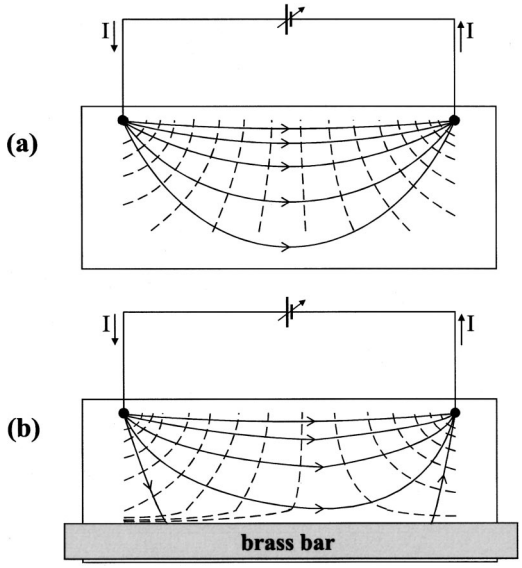

Fig. 3. Equipotential (dashed lines) and electric field (solid lines) maps for two current electrodes placed at 24 cm separation (equivalent to a Wenner array with 8 cm *a*-spacing) for (a) conductive sheet without bar and (b) conductive sheet with bar placed at a depth of 8 cm. Adjacent equipotential lines differ by 0.5 V. The same current, 500 μA, was used for both cases.

sure the changes that occur with changing layer depth. Also, differences between horizontal and vertical layers are investigated.

II. LABORATORY

Our experiment uses materials from the Charge, Equipotential and Field Mapper kit available from Pasco.[6] The kit includes 23 cm×30 cm conductive paper sheets with a printed grid, regular white paper sheets with a similar grid, and larger 30 cm×46 cm conductive sheets without a grid. In addition, the kit includes silver paint for drawing conducting distributions and pushpins to connect the conducting distributions to the wires from the power supply.

Horizontal layers. To model a Wenner array over horizontal layers, we use the large conductive paper with pushpins inserted on prepainted silver pads at the points where measurements will be taken, as shown in Fig. 1. The pushpins represent current and potential electrodes and the top of the paper represents the surface of the earth. To simulate a lower resistivity layer at some depth (for example, water saturated sediment) we use a 1 in.×1 in.×20 in. brass bar that can be moved to any desired position below the pushpins. The brass bar is first placed at the bottom of the paper, a distance of 28 cm from the pushpins, and a Wenner spread is conducted for each of the possible *a*-spacings. The current is held constant at 100 μA for the entire experiment. The brass bar is then moved upward to depths of 24, 20, 16, 12, 8, 6, 4, and 2 cm and subsequent Wenner spreads are conducted for each new position.

Sample data for the electric potential difference (ΔV) between the inner electrodes as a function of *a*-spacing are shown in Fig. 2. The natural logarithm of ΔV has been plotted to emphasize relative changes. For clarity, data for suc-

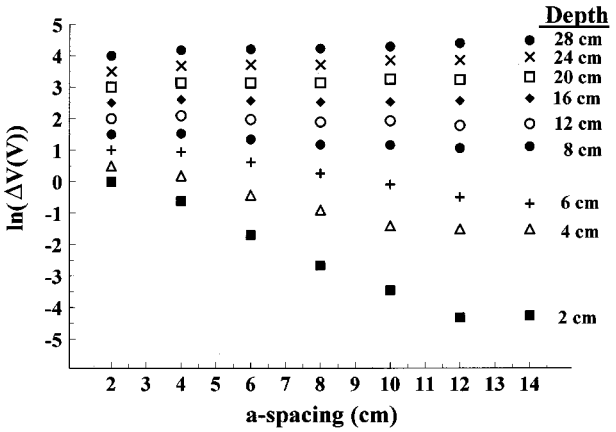

Fig. 2. Electric potential difference (ΔV) data for expanding Wenner spreads on paper with adjustable brass bar. Each group of symbols represents an individual expanding spread conducted for a particular bar position (depth). For clarity, data for successive bar depths have been shifted by 0.5 vertically to separate them on the graph.

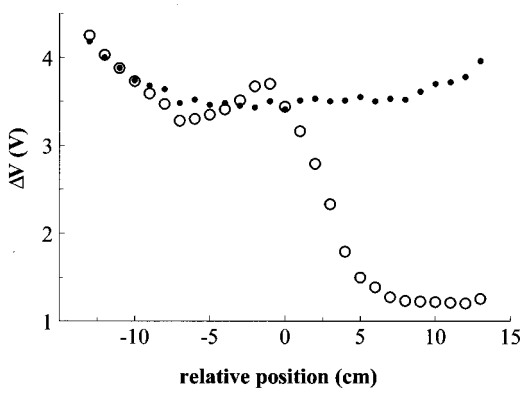

Fig. 4. Electric potential difference (ΔV) data for a constant separation traverse on paper. Open large circles represent data for a single conducting sheet on the left half of the traverse and five conducting sheets on the right half of the traverse. Closed small circles represent data for a single conducting sheet for the entire traverse. The position of the center of the electrode spread relative to the center of the traverse is plotted.

cessive bar depths have been shifted vertically by 0.5 to separate them on the graph. For deeper bar depths, from 16 to 28 cm for example, ΔV does not change appreciably with changes in a-spacing. However, for shallower depths, ΔV decreases dramatically with increases in a-spacing. For a depth of 2 cm, there is a reduction of ΔV by two orders of magnitude over the spread. All of these results are consistent with the notion that a larger percentage of the current travels to greater depths at larger a-spacings and that the lower resistivity layer (the brass bar) is only sampled when the a-spacing begins to approach the depth to the layer. From the students' standpoint, an interesting aspect of this experiment is that the resistivity of the brass bar is affecting the overall resistivity although the pushpins never come in contact with the brass bar. Through follow-up questions we emphasize this point and explain the usefulness of this geophysical method as a noninvasive means of gathering information about subsurface layers.

On closer examination, the Wenner spread data show a slight increase in ΔV with increasing a-spacing for spreads when the bar is deep, between 20 and 28 cm. In fact, with no bar present, ΔV increases by 50% for a-spacings from 2 to 14 cm. Therefore, the data deviate from the theoretically derived result that ΔV is independent of a-spacing for a homogeneous subsurface. The main reason for this deviation is that the paper dimensions are not infinite and the restriction of the current to within the paper boundaries increases the measured electric potential difference, especially for a-spacings that approach the width of the paper. The limitations of the paper boundaries do not affect the qualitative results significantly, however, and the effect of the brass bar is clearly seen, especially when plotted on a logarithmic scale.

To gain a more precise understanding of the reason for the changing ΔV due to the brass bar, students set up a Wenner spread on the smaller conductive paper with grids. They then record the electric potential relative to the negative current electrode (which we designate as zero electric potential) at a series of grid locations for one particular a-spacing, with and without the brass bar. They use a bar depth of 8 cm and a-spacing of 8 cm so that the influence of the bar is significant. The students then map the equipotential lines and the perpendicular electric field lines between the two current electrodes. Emphasis is placed on displaying a higher density of electric field lines where the change in the equipotential lines occurs over the shortest distance. Equipotential and electric field lines are shown in Fig. 3 for the Wenner spread with and without the brass bar. There are two main differences in the data with the brass bar present. First, the spacing between adjacent equipotential lines is greater near the center of the grid. Second, the curvature of the equipotential lines is greater, especially near the position of the brass bar. Both results are consistent with a reduced density of electric field lines and a greater curvature of the electric field lines near the brass bar. A reduced density of electric field lines in the upper layer is indicative of a greater percentage of the current traveling through the lower resistivity layer. In essence, the redistribution of the current toward the lower resistivity layer results in a smaller electric potential difference between the inner electrodes at the top of the higher resistivity layer. The lower measured electric potential leads to a lower measured apparent resistivity and indirectly indicates the presence of the brass bar.

Vertical layers. Another type of resistivity spread in common use is known as a constant separation traverse.[4] The technique is most useful in the vicinity of vertical or highly sloping layers. A Wenner spread is used and the a-spacing is kept constant while the center of the spread is moved. To facilitate modeling this technique on paper, the large conductive paper is used and pushpins are inserted at the top of the paper every centimeter. Underneath the right half of the sheet of paper, several more conductive sheets are inserted to simulate a transition from high-resistivity to low-resistivity vertical layers. To best visualize the essential features of the traverse, an a-spacing of 6 cm suffices. Starting from the left side of the paper, the traverse progresses by shifting each electrode equal increments of 1 cm until the right side of the paper is reached.

In Fig. 4, the electric potential difference between inner electrodes is plotted as a function of the position of the center of the electrode spread relative to the position of the center line separating the high- and low-resistivity halves. The layers on the left and the right consisted of one and five conductive sheets, respectively. For these data, the current was held constant at 300 μA. Plotted for comparison are data for the same constant separation traverse over homogeneous ground (one conductive sheet). The control data show the same boundary effects as for the Wenner data in Fig. 2. Compared to these control data, the other data show a clear difference in ΔV between the extreme left and right ends of the traverse, as expected. If the data are corrected for the edge effects, the resistivities at the extreme left and right ends of the traverse differ by a factor of 4.9, very close to the expected 5:1 ratio. Students can therefore use this calculation to determine the relative number of conducting sheets. In addition, there are two distinct cusps in the data at positions -7 and -1 cm. The first occurs when the lead current electrode crosses the vertical contact into the lower resistivity layer and the second occurs when the lead potential electrode crosses into the lower resistivity layer. This characteristic signature is often used to locate the position of the vertical contact, emphasizing the usefulness of this technique.[4] A complete mathematical analysis of the origin of this curve is given by Telford *et al.*[5]

ACKNOWLEDGMENTS

This work was funded in part by NSF Grant No. 9950260. The authors would like to thank Mark Lord and Ginny Peterson for useful discussions.

[a]Electronic mail: vndrvrt@wcu.edu
[b]Present address: Department of Physics, University of Tennessee, Knoxville, TN.

[1]Brian Avants, Dustin Soodak, and George Ruppeiner, "Measuring the electrical conductivity of the earth," Am. J. Phys. **67**, 593–598 (1999).
[2]Ana Osella, Gabriel Chao, and Federico Sánchez, "How to detect buried structures through electrical measurements," Am. J. Phys. **69**, 455–461 (2001).
[3]Rhett Herman, "An introduction to electrical resistivity in geophysics," Am. J. Phys. **69**, 943–952 (2001).
[4]H. Robert Burger, *Exploration Geophysics of the Shallow Subsurface* (Prentice–Hall, Englewood Cliffs, NJ, 1992), pp. 241–316.
[5]W. M. Telford, L. P. Geldart, R. E. Sheriff, and D. A. Keys, *Applied Geophysics* (Cambridge U.P., London, 1976), pp. 632–701.
[6]Pasco Scientific, 10101 Foothills Blvd., Roseville, CA 95747-7100, (916)-786-3800.

Undergraduate experiment to measure the speed of sound in liquid by diffraction of light

Diego A. Luna,[a] Mariano A. Real, and Débora V. Durán
Facultad de Ciencias Exactas y Naturales, Universidad de Buenos Aires, Pabellón II, Ciudad Universitaria 1428 Capital Federal, Argentina

(Received 4 October 2001; accepted 10 May 2002)

Diffraction of light by an ultrasonic phase grating enables a direct measurement of the wavelength of acoustic waves in liquids. If the acoustic frequency is known independently, it can be combined with the measured acoustic wavelength to determine the speed of sound in liquid. The method of Debye and Sears based on a visual display of the diffraction pattern on a distant screen is used. Measurements carried out with a He–Ne laser and an ultrasonic nebulizer provide an excellent experiment for an undergraduate laboratory with a minimum of equipment. A sound velocity of 1536 m/s with an uncertainty of 1% is obtained for distilled water. © *2002 American Association of Physics Teachers.*
[DOI: 10.1119/1.1491263]

I. INTRODUCTION

The diffraction of light by ultrasound in a liquid provides a direct means for determining the velocity of sound in a liquid. The pressure variations of the sound wave as it propagates through the liquid changes the refractive index. This makes the liquid act as a grating that will diffract a light beam incident on the liquid in a direction normal to the propagation direction of the sound wave. The spatial periodicity of the density variation is a direct measure of the acoustic wavelength.

In this note, the Debye and Sears[1,2] method is used to measure the speed of sound in distilled water. The main purpose of this work is to describe an inexpensive experiment to measure the speed of sound in liquid.

II. EXPERIMENT

The experimental arrangement used by Debye and Sears[1,2] is similar to the case in which an ordinary ruled grating is studied. In this work, a 632.8 nm wavelength Melles Griot 05-LHR-141 He–Ne laser is used as a 4 mW light source to produce the diffraction pattern on a distant screen. To produce ultrasound waves in a liquid, the piezoelectric transducer of an ultrasonic nebulizer has been used. An old ultrasonic nebulizer can usually be obtained at a pharmacy; it's a nebulizer that has a piezoelectric transducer connected to a radio-frequency generator (in our case a 25 MHz one) that works at ultrasonic frequencies (as the name indicates). The advantage of the ultrasonic nebulizer is that no circuit design is needed and it's inexpensive. A test tube, whose bottom was previously cut out, has been glued around the piezoelectric disk of the nebulizer. To make it possible for us to change the effective length of the tube, a piston of the same diameter of the test tube was used. The optical arrangement of the apparatus is shown in Fig. 1. A plane acoustic wave front is sent through the liquid at a right angle to the direction of propagation of light. After passing through the liquid in the test tube, the laser beam turns into a divergent wave front as shown in Fig. 2.

The angular positions of the diffraction maxima for a liquid grating were found by Raman and Nath[3] to be given by

$$a \sin \phi_m = m\lambda \quad (m = 0,1,2,...), \tag{1}$$

where ϕ_m is the angle corresponding to the mth order diffracted beam, a is the spatial periodicity of the grating, and λ is the wavelength of light in air. It is the same equation as the corresponding one for a ruled grating, but the central maximum is not necessarily the brightest.[4,5] This formula is valid for traveling and standing sound waves, whether or not the Doppler effect is taken fully into account.[6]

During the experiment, the liquid is considered to be a nondispersive medium. In this case, the dispersion relation is given by

$$\nu_s = \Lambda \upsilon, \tag{2}$$

where ν_s is the speed of sound in the liquid, Λ is the acoustic wavelength, and υ is the acoustic frequency. The Raman–Nath model explains that the pressure waves generated by the nebulizer can be considered as a grating, and the acoustic wavelength Λ is the spatial periodicity of the grating. Combining Eqs. (1) and (2), one obtains

$$\nu_s \sin \phi = m\lambda \upsilon. \tag{3}$$

The frequency of the acoustic waves, υ, generated by the piezoelectric disk was measured directly by a Tektronix TDS210 oscilloscope and found to be 26.5 ± 0.5 MHz.

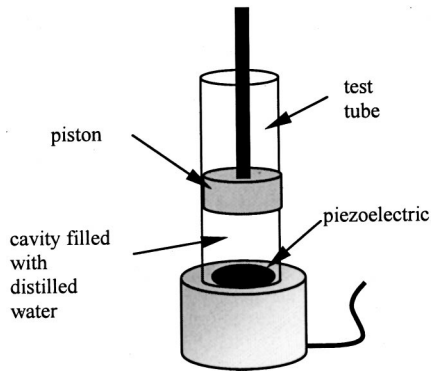

Fig. 1. Optical system for observing the diffraction of light by ultrasonic waves in liquid.

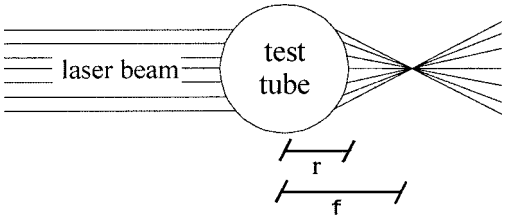

Fig. 2. Geometrical description of the wave front. Here r is the radius of the tube and f the distance to the focus.

Equation (3) predicts the angular positions of the maxima in a diffraction pattern generated by ultrasound in liquids. Here it has been used to determine the speed of sound in distilled water.

A whiteboard placed at a distance of 9.36 ± 0.04 m was used as an observation screen. The long distance was necessary to distinguish the different diffraction orders. On the screen, horizontal lines were obtained instead of the characteristic pattern of points, because the water-filled test tube acted as a cylindrical lens, as shown in Fig. 2. The diffraction pattern was recorded by tracing it with a ruler on the whiteboard. The distance between orders was then measured. A photograph of the diffraction pattern obtained by passing the He–Ne laser beam through distilled water is shown in Fig. 3.

The same experiment has been repeated several times, and a straight line has been fitted to the sine of the diffraction angles. This regression fit is shown in Fig. 4, where the value of the slope indicates the speed of sound in the liquid, in this case 1536 m/s with an uncertainty of $\pm 1.1\%$. This value is consistent with the value of 1541.4 m/s given in Ref. 6.

A final consideration: For the liquid to act as a grating, the laser beam must illuminate several periods of it. In this experiment the incident light beam was about 1.5 mm wide, so that only two or three periods of the acoustic wave train were illuminated, enough to produce the phenomenon of a grating. If other liquids of lower density were used, more periods of the acoustic wave train would be illuminated and more diffraction maxima would be seen on the screen, thus improving experimental accuracy.[7]

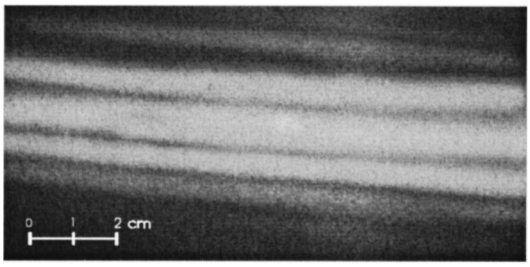

Fig. 3. Photograph of the diffraction pattern obtained.

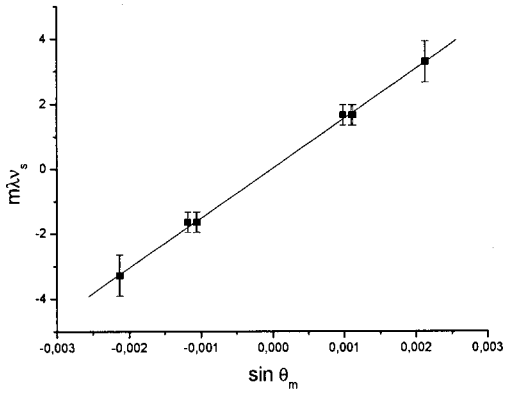

Fig. 4. Linear regression of the collected data.

III. CONCLUSION

In this paper the Raman–Nath model for an acoustic grating has been verified. The experimental method of Debye and Sears was effective and easy to arrange. Although only two periods of the acoustic wave train were illuminated, good diffraction results were obtained.

This is an example of an elementary acousto-optics experiment that can be carried out in an undergraduate laboratory. Considering the equipment used, it provides a precise value of the speed of sound in liquids.

ACKNOWLEDGMENTS

We are grateful to C. Iemmi, M. Irigoyen, and M. Paulozzi for stimulating discussions and assistance in the course of the experiment. This experiment is a work of an undergraduate physics laboratory at the Universidad de Buenos Aires.

[a]Electronic mail: diega@xlnet.com.ar

[1]P. Debye and F. W. Sears, "Scattering of light by supersonic waves," Proc. Natl. Acad. Sci., Wash. **18**, 409–413 (1935).

[2]L. Bergmann, *Ultrasonics and their Scientific and Technical Applications* (Wiley, New York, 1938), pp. 59–71.

[3]C. V. Raman and N. S. Nagendra Nath, "The diffraction of light by high frequency sound waves," Proc. Ind. Acad. Sci. (A) **2**, 406–413 (1935).

[4]P. Kang and F. C. Young, "Diffraction of laser light by ultrasound in liquid," Am. J. Phys. **40**, 697–703 (1972).

[5]J. F. Neeson and S. Austin, "Sound velocity and diffraction intensity measurements based on Raman–Nath theory of the interaction of light and ultrasound," Am. J. Phys. **43**, 984–986 (1975).

[6]F. Crawford, Jr., *Waves*, Berkeley Physics Course Vol. 3 (Reverté, Barcelona, 1994), Chap. 4, pp. 169–187.

[7]*Handbook of Chemistry and Physics*, 78th ed., Sec. 3, p. 157, and Sec. 14, p. 37.